Spectroscopic Evidence of Luttinger Liquid Behavior in a Single-Layer Nickelate

Yinqi Hu,[1] Yidian Li,[1] Xian Du,[2] Wenxuan Zhao,[1] Kaiyi Zhai,[1] Senyao Zhang,[1] Jiawei Shao,[1] Mingxin Mao,[1] Houke Chen,[3] Jieyi Liu,[3,4] Donghui Lu,[5] Makoto Hashimoto,[5] Fangyuan Zhu,[6] Zhengtai Liu,[6] Dawei Shen,[7] Yaobo Huang,[6] Zhongkai Liu,[8,9] D. Prabhakaran,[3] Yanpeng Qi,[8,9,10,*] Yilin Wang,[11,12,13,†] Yulin Chen,[3,8,9,‡] and Lexian Yang[1,14,§]

[1]*Department of Physics, State Key Laboratory of Low Dimensional Quantum Physics, Tsinghua University, Beijing 100084, China*
[2]*Department of Applied Physics, Yale University, New Haven, Connecticut 06511, USA*
[3]*Department of Physics, Clarendon Laboratory, University of Oxford, Parks Road, Oxford OX1 3PU, United Kingdom*
[4]*Diamond Light Source, Harwell Science and Innovation Campus, Didcot OX11 0DE, United Kingdom*
[5]*Stanford Synchrotron Radiation Lightsource, SLAC National Accelerator Laboratory, Menlo Park, California 94025, USA*
[6]*Shanghai Synchrotron Radiation Facility, Shanghai Advanced Research Institute, Chinese Academy of Sciences, Shanghai 201210, China*
[7]*National Synchrotron Radiation Laboratory and School of Nuclear Science and Technology, University of Science and Technology of China, Hefei 230026, China*
[8]*School of Physical Science and Technology, ShanghaiTech University, Shanghai 201210, China*
[9]*ShanghaiTech Laboratory for Topological Physics, Shanghai 200031, China*
[10]*Shanghai Key Laboratory of High-resolution Electron Microscopy, ShanghaiTech University, Shanghai 201210, China*
[11]*School of Emerging Technology, University of Science and Technology of China, Hefei 230026, China*
[12]*New Cornerstone Science Laboratory, University of Science and Technology of China, Hefei 230026, China*
[13]*Hefei National Laboratory, University of Science and Technology of China, Hefei 230088, China*
[14]*Frontier Science Center for Quantum Information, Beijing 100084, China*

(Received 31 December 2025; revised 21 July 2026; accepted 2 October 2026; published 10 November 2026)

The discovery of high-temperature superconductivity in bilayer and trilayer nickelates has spurred intense interest in the Ruddlesden-Popper nickelates, yet the fundamental properties of the NiO_2 layer remain obscured by interlayer coupling. It is therefore imperative to investigate the electronic properties of their single-layer counterpart—though not superconducting—to isolate the intrinsic physics of the Ni-O layer. In this work, we present a systematic study of the single-layer nickelate $La_{1.4}Sr_{0.6}NiO_4$ using high-resolution angle-resolved photoemission spectroscopy and theoretical calculations. We reveal strong electron correlation effects manifested by high-energy kinks in band dispersions and a pronounced orbital-dependent band renormalization. Interestingly, we observe a quasi-one-dimensional electronic structure characterized by straight Fermi surface sheets along the diagonal momentum directions. Such a squarelike Fermi surface topology facilitates non-Fermi-liquid behavior consistent with the Luttinger liquid model, as evidenced by the power-law spectral function, robust temperature scaling, and spectroscopic features reminiscent of spin-charge separation. Our results therefore not only point toward an exotic Luttinger liquid phase emerging from the unexpected dimensional reduction in an intrinsically quasi-two-dimensional nickelate but also provide a new perspective for understanding the intriguing physics in multilayer nickelates.

DOI: 10.1103/744w-ln1x

Subject Areas: Condensed Matter Physics, Strongly Correlated Materials, Superconductivity

*Contact author: qiyp@shanghaitech.edu.cn
†Contact author: yilinwang@ustc.edu.cn
‡Contact author: yulin.chen@physics.ox.ac.uk
§Contact author: lxyang@tsinghua.edu.cn

Published by the American Physical Society under the terms of the Creative Commons Attribution 4.0 International license. Further distribution of this work must maintain attribution to the author(s) and the published article's title, journal citation, and DOI.

I. INTRODUCTION

Nickelates, long regarded as structural and electronic analogs of cuprates, have recently emerged as a compelling platform for exploring high-temperature superconductivity [1–7]. In particular, layered nickelates in Ruddlesden-Popper (RP) phase demonstrate unconventional superconductivity, with critical temperature exceeding the liquid-nitrogen boiling point [8–15]. These breakthroughs have spurred a surge of investigations aimed at unraveling the unique electronic mechanisms that underpin their superconducting and strongly correlated behaviors [16–18]. Among the many theoretical and experimental findings, the non-Fermi-liquid behavior of the RP-phase nickelates, such as $La_3Ni_2O_7$ and $La_4Ni_3O_{10}$, is of particular interest [19–26]. Although the origin of this anomalous behavior remains elusive, its resolution is essential to advancing our understanding of the electronic landscape and the nature of unconventional superconductivity in RP-phase nickelates.

Notably, Fermi surfaces with large flat segments have been widely observed in various nickelate systems, including bilayer $La_3Ni_2O_7$ and trilayer $La_4Ni_3O_{10}$ [23,27,28], the alternating monolayer-trilayer $La_3Ni_2O_7$ [29], and $LaNiO_3$ thin films [30,31]. Such a Fermiology is reminiscent of quasi-one-dimensional (1D) electronic systems [32,33], except that the parallel flat segments in these compounds run along two orthogonal momentum directions, forming a squarelike geometry. Theoretical studies have explored the implications of the square Fermi surface based on a square lattice model dominated by nearest-neighbor hopping [Figs. 1(a) and 1(b)], suggesting its potential connection to density-wave instability and unconventional superconductivity [34–36]. The square geometry is particularly intriguing, as it gives rise to non-Fermi-liquid behavior [34–36], resonating with Anderson's hypothesis that the 2D electron gas behaves like a Luttinger liquid (LL) in 1D rather than a Fermi liquid [37]. Nevertheless, experimental validation of this connection remains sparse. Nickelates offer a rare opportunity to explore this intriguing problem. However, the strong interlayer interaction and octahedral distortion in multilayer nickelates complicate the Fermi surface structure and obscure the intrinsic physics of the Ni-O square lattice. Consequently, their single-layer counterpart offers an

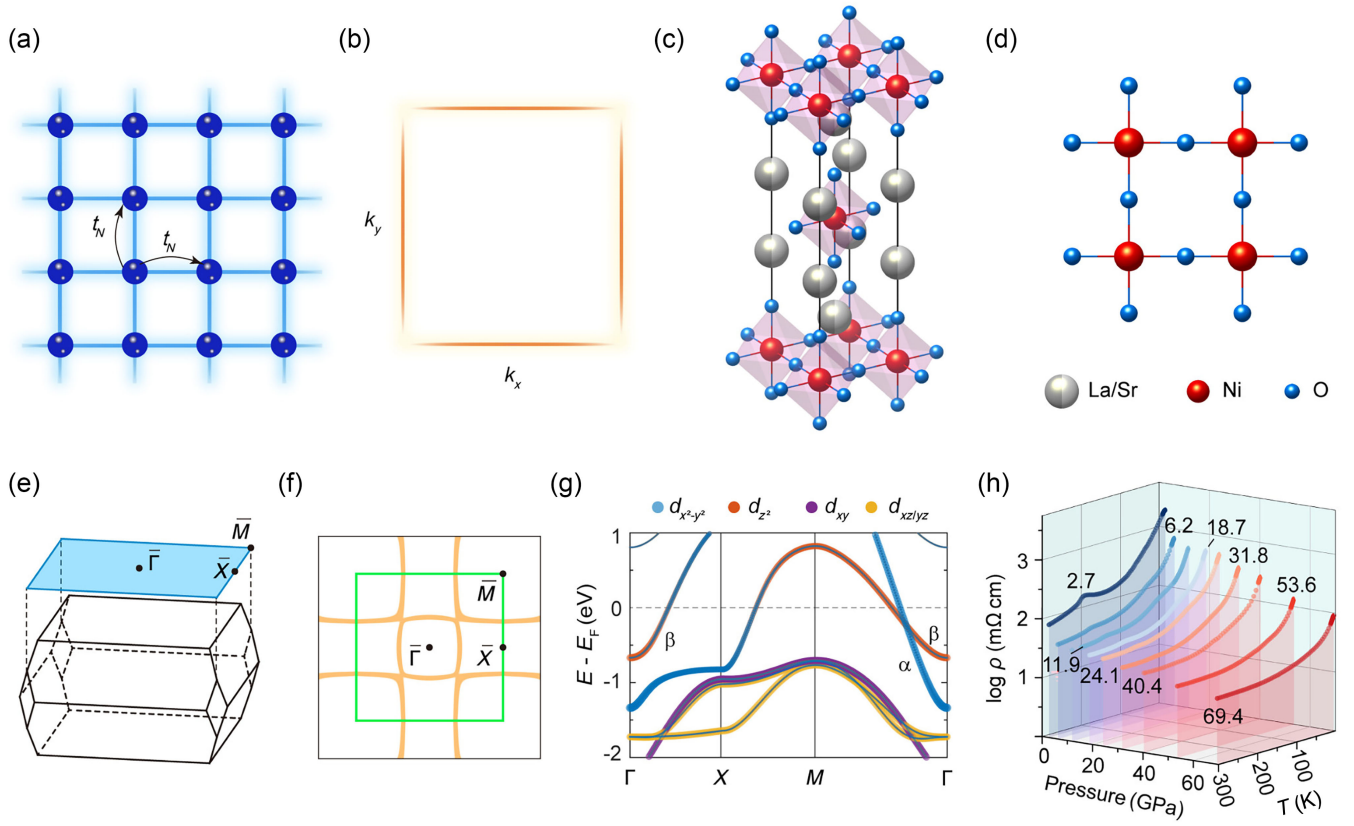


FIG. 1. Basic properties of $La_{1.4}Sr_{0.6}NiO_4$. (a) Schematic illustration of a square lattice with nearest-neighbor hopping dominating the low-energy electronic excitations. (b) Schematic of the square Fermi surface of the two-dimensional lattice model in (a). (c) Illustration of the crystal structure of $La_{2-x}Sr_xNiO_4$ with Ni-O layers separated by La-O layers. (d) The Ni-O layer as the basic construction unit in nickelate superconductors. (e) 3D Brillouin zone of $La_{2-x}Sr_xNiO_4$ and its surface projection. (f) Fermi surface of $La_{1.4}Sr_{0.6}NiO_4$ calculated by DFT. (g) DFT-calculated orbital-projected band structure of $La_{1.4}Sr_{0.6}NiO_4$. (h) Temperature-dependent resistivity under different pressures.

optimal route to disentangle the pivotal role of Ni-O planes and interlayer interaction in shaping the electronic ground states, motivating a focused investigation of the intrinsic physics within the Ni-O layer.

In this work, we present a systematic study of the single-layer RP-phase nickelate $La_{1.4}Sr_{0.6}NiO_4$ using angle-resolved photoemission spectroscopy (ARPES) and *ab initio* calculations to elucidate the intrinsic physics of the Ni-O layer. We observe strong electron correlation effects manifested by high-energy kinks resembling the band dispersion of cuprates, alongside pronounced orbital-dependent band renormalization resulting from strong Coulomb interaction and Hund's coupling. Prominently, our work reveals a quasi-1D electronic structure along orthogonal momentum directions, forming flat Fermi surface segments. Such a squarelike Fermi surface engenders the non-Fermi-liquid behavior that follows the LL model, as evidenced by a power-law spectral function, robust temperature scaling behavior, and the spectroscopic features suggestive of spin-charge separation [34–36]. Our findings therefore provide spectroscopic evidence consistent with LL behavior, which originates from an unexpected reduction in the dimensionality of the electronic structure within a quasi-two-dimensional system. These results establish the single-layer nickelate as an important platform for investigating the interplay among electron correlation, Hund's coupling, and dimensionality in multi-orbital electronic systems [38–40], which further provide important insights for deciphering anomalous electronic properties of multilayer nickelates.

II. RESULTS

Figure 1(c) schematically illustrates the crystal structure of $La_{2-x}Sr_xNiO_4$ in the RP phase. It comprises alternating layers of corner-sharing NiO_6 octahedra and La/Sr atomic layers, periodically stacked along the c axis. The out-of-plane tilt of the NiO_6 octahedra is suppressed by replacing La with Sr. For $x > 0.21$, $La_{2-x}Sr_xNiO_4$ crystallizes in the space group $I4/mmm$ [41]. As presented in Fig. 1(d), the square Ni-O plane is similar to the Cu-O plane in cuprates, with nearest-neighbor Ni atoms connected by in-plane O atoms. Figure 1(e) shows the 3D Brillouin zone and its surface projection with high-symmetry points indicated. The Fermi surface of $La_{1.4}Sr_{0.6}NiO_4$ calculated by density-functional theory (DFT) consists of nearly parallel sheets extending along $\bar{\Gamma}\,\bar{X}$ [Fig. 1(f)], in contrast to that of $La_3Ni_2O_7$ with rounded-square or circular Fermi pockets [23,42]. The DFT calculation predicts a metallic band structure where the energy bands crossing E_F are contributed by $d_{x^2-y^2}$ and d_{z^2} orbitals [Fig. 1(g)], similar to $La_3Ni_2O_7$ and $La_4Ni_3O_{10}$ [23,27,28,43]. Nevertheless, the d_{z^2} orbital does not show a flat band but quickly disperses across E_F. Figure 1(h) displays temperature-dependent resistivity under selected pressures. At low temperatures, $La_{1.4}Sr_{0.6}NiO_4$ exhibits no indication of superconductivity up to 69 GPa, which underscores the critical role of interlayer hopping in the emergence of superconductivity in bilayer and trilayer nickelates [42,44–47]. At 2.67 GPa, the resistivity curve shows an upturn around 220 K, which may be related to charge or spin ordering [48,49].

Figure 2 presents the basic band structure of $La_{1.4}Sr_{0.6}NiO_4$ measured with high-resolution ARPES. The constant-energy contours at different binding energies consist of parallel line segments along $\bar{\Gamma}\,\bar{X}$ [Fig. 2(a)]. While in overall agreement with the DFT calculation in Fig. 1(f), the experimental Fermi surface appears straighter, resembling the electronic structure of quasi-1D electronic systems [32,33]. The Fermi surface of $La_{1.4}Sr_{0.6}NiO_4$ can be regarded as two sets of parallel lines with weak hybridization at the crossing points [Fig. 2(b)], which is different from those of $La_3Ni_2O_7$ and $La_4Ni_3O_{10}$ with a circular electron pocket around $\bar{\Gamma}$ (also see Supplemental Material [50]). The invariance of the momentum distribution curves (MDCs) along the Fermi surface [indicated by the white rectangle in Fig. 2(b)] confirms the straightness of the parallel Fermi surface sheets [Fig. 2(c)]. Moreover, the Fermi momenta and Fermi velocities show minor dependence on the momentum [Fig. 2(d)], reinforcing the quasi-1D character of the electronic structure of $La_{1.4}Sr_{0.6}NiO_4$.

Figures 2(e)–2(h) present the band dispersions along high-symmetry directions. We observe two bands near E_F, which are contributed by the $d_{x^2-y^2}$ and d_{z^2} orbitals, according to the DFT calculations [Fig. 2(e)]. In contrast to $La_3Ni_2O_7$ and $La_4Ni_3O_{10}$, the top of the d_{z^2} band is far above E_F, leaving no flat band near E_F. In the experiments, the α band derived from the $d_{x^2-y^2}$ orbital disperses down to −1 eV, below which the spectra are dominated by strong and slowly dispersing features. The DFT-calculated band structures are overlaid for comparison, showing overall agreement between the experiments and calculated results. The α band is well reproduced by the calculation, while a substantial renormalization by a factor of about 3 is required for the calculated β band that is dominated by the d_{z^2} orbital character near the $\bar{\Gamma}$ point, suggesting an orbital-dependent electron correlation effect (see Supplemental Material [50]), in line with multilayer nickelates $La_3Ni_2O_7$ and $La_4Ni_3O_{10}$. Compared with $La_{1.4}Sr_{0.6}NiO_4$, the band renormalization in $La_3Ni_2O_7$ and $La_4Ni_3O_{10}$ is enhanced roughly by a factor of 2 due to interlayer interaction. Assuming a comparable Ni valence, this points to an important role of interlayer electron correlation effect in the physics of multilayer compounds [51].

Interestingly, the band dispersion around $\bar{X}$ comprising a mixture of the two orbitals [Fig. 1(g)] shows a pronounced kinklike structure around −260 meV [Figs. 2(g) and 2(h)], as better visualized in the enlarged plots in Figs. 3(a) and 3(b). Such a "waterfall-like" feature in the band dispersion has been commonly observed in many correlated materials and is widely regarded as a manifestation of strong electron correlation [43,52–59]. By fitting the MDCs at different

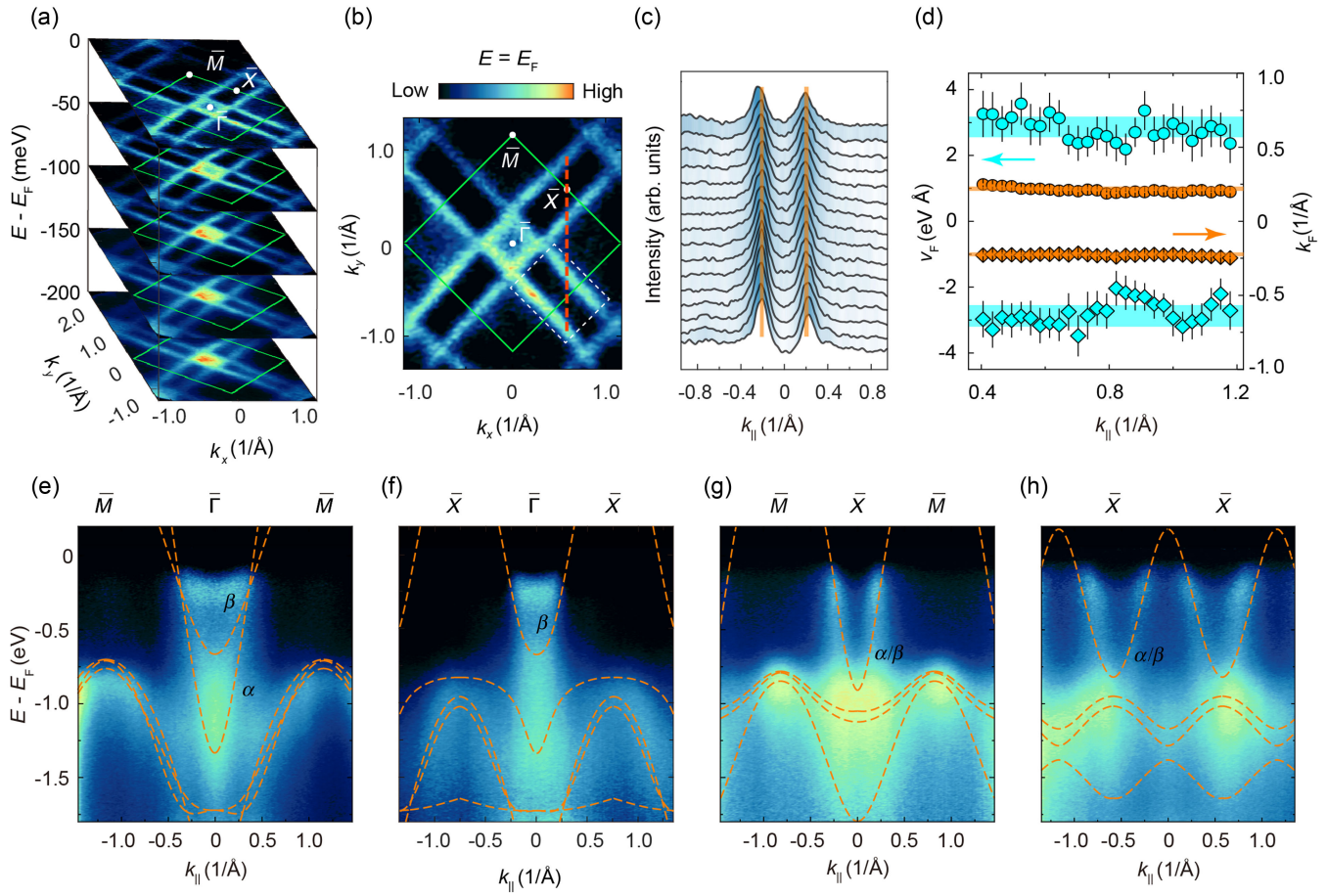


FIG. 2. Basic electronic structure of $La_{1.4}Sr_{0.6}NiO_4$. (a) Stacking plot of constant-energy contours at selected binding energies. The green lines indicate the first Brillouin zone. (b) Fermi surface measured by integrating ARPES intensity in an energy window of 40 meV around the Fermi level (E_F). (c) Stacking plot of momentum-distribution curves at E_F in the momentum region as indicated by the white dashed rectangle in panel (b). (d) Fermi momenta and Fermi velocity as functions of the momentum in the white dashed rectangle in panel (b). (e)–(h) Band dispersions along different momentum directions. The momentum direction of panel (h) is indicated by the red dashed line in (b). DFT-calculated band structures (orange dashed lines) are overlaid for comparison. Data in (e) and (h) were collected using linear-horizontally- (LH) polarized photons at 153 eV, while data in (a), (b), (f), and (g) were collected using LH-polarized photons at 182 eV. All data were collected at 15 K.

binding energies to Lorentzian functions (see Supplemental Material [50]), we extract the electron self-energy of $La_{1.4}Sr_{0.6}NiO_4$. The imaginary part of the electron self-energy gradually increases with the binding energy, while the real part exhibits a maximum at approximately 260 meV below the Fermi energy [Figs. 3(c) and 3(d)], which is far beyond the energy range of normal lattice vibrations. The electron self-energies of cuprate $Bi_{1.74}Pb_{0.38}Sr_{1.88}CuO_{6+\delta}$ (Bi2201) are replotted from Ref. [52] for comparison. The comparable onset energy of the waterfall-like feature in single-layer nickelate and cuprate suggests their similar electron correlation effects [54], although the electron correlation effect is further modulated by Hund's coupling in nickelates (see Supplemental Material [50]).

Having established basic electronic structure and electron correlation effects, we now focus on the spectral features in the vicinity of E_F. We notice that the spectral weight is significantly suppressed upon approaching E_F (Figs. 2 and 3), a hallmark of non-Fermi-liquid behavior. In Fig. 4, we scrutinize this non-Fermi-liquid behavior based on the LL model, motivated by the quasi-1D electronic structure and squarelike Fermi surface of $La_{1.4}Sr_{0.6}NiO_4$. Figure 4(a) presents the temperature-dependent ARPES spectra measured using laser ARPES with improved resolutions. Consistent with the spectra measured with synchrotron-based ARPES, no clear quasiparticle peak is observed near E_F, similar to the results in $La_3Ni_2O_7$ and $La_4Ni_3O_{10}$ [23,27,28]. Figure 4(b) compares ARPES spectra of $La_{1.4}Sr_{0.6}NiO_4$ with those of prototypical Fermi liquid and LL materials. $La_{1.4}Sr_{0.6}NiO_4$ is clearly distinct from the polycrystalline gold, a reference Fermi liquid with a well-defined Fermi edge. Instead, it closely resembles the prototypical quasi-1D LL materials [32,33,60].

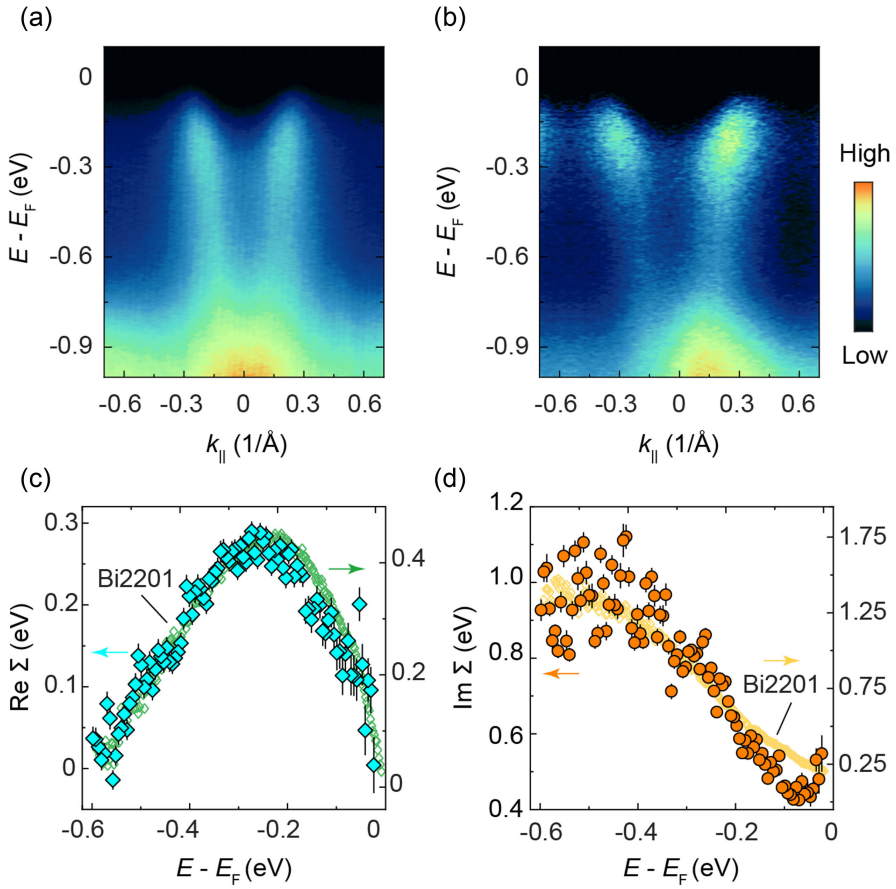


FIG. 3. Electron correlation effect of $La_{1.4}Sr_{0.6}NiO_4$. (a),(b) Band dispersions along $\bar{X}\,\bar{M}$ and the red dashed line in Fig. 2(b) measured at 15 K. Data were collected using LH-polarized photons at 163 and 153 eV, respectively. (c),(d) Real and imaginary parts of electron self-energy extracted from band dispersion in (b), with real and imaginary parts of Bi2201 overlaid for comparison. Data of Bi2201 were collected at 20 K with 22.5 eV photons according to Ref. [52].

To quantify the LL behavior of $La_{1.4}Sr_{0.6}NiO_4$, we fit the experimental data to the LL model at finite temperature [33]:

$$\rho(\epsilon, T) \propto T^{\alpha}\mathrm{Re}\left[(2i)^{\alpha+1}B\left(\frac{\alpha+1-[(i\epsilon)/\pi]}{2}, -\alpha\right)\right],$$

where $\rho(\epsilon, T)$ represents the LL spectral function, $\epsilon = (E - E_F)/k_BT$ is the scaled energy with k_B the Boltzmann constant. B is the beta function, and α represents the LL anomalous exponent. Within the Luttinger-liquid framework, $\alpha = 0$ corresponds to the noninteracting Fermi-liquid-like limit, whereas electron correlations lead to a finite exponent $\alpha > 0$, producing a power-law suppression of the spectral weight near the Fermi level. As shown in Fig. 4(c), the ARPES data of $La_{1.4}Sr_{0.6}NiO_4$ are well described by the LL model over a wide temperature range from 21 to 185 K, yielding a temperature-independent exponent $\alpha \approx 0.39 \pm 0.04$ (see Supplemental Material [50]). The LL property can be independently verified through its characteristic scaling behavior with the temperature. That is, the integrated ARPES spectra scaled by T^{α} should be temperature independent, which is convincingly verified in Fig. 4(d) with $\alpha \approx 0.37$. Furthermore, the LL model predicts a linear dependence of $\log[I(E_F)]$ on $\log T$ with the slope corresponding to the LL exponent α, where I represents the spectral intensity. This linear relationship with $\alpha \approx 0.38$ is demonstrated in Fig. 4(e), consistent with both the model fitting and the scaling analysis. Remarkably, we observe two band dispersions at the $\bar{X}$ point, compared to the single band predicted by DFT calculations, as better visualized by the curvature plot [Fig. 4(f)]. This result is in close analogy to the previous reports of spin-charge separation [61–64], suggesting that these two bands correspond to separate dispersion branches of spinon and chargon. Based on the above experimental findings, our data point toward LL behavior of $La_{1.4}Sr_{0.6}NiO_4$, which is associated with the quasi-1D electronic structure hidden within its nominally two-dimensional crystal structure.

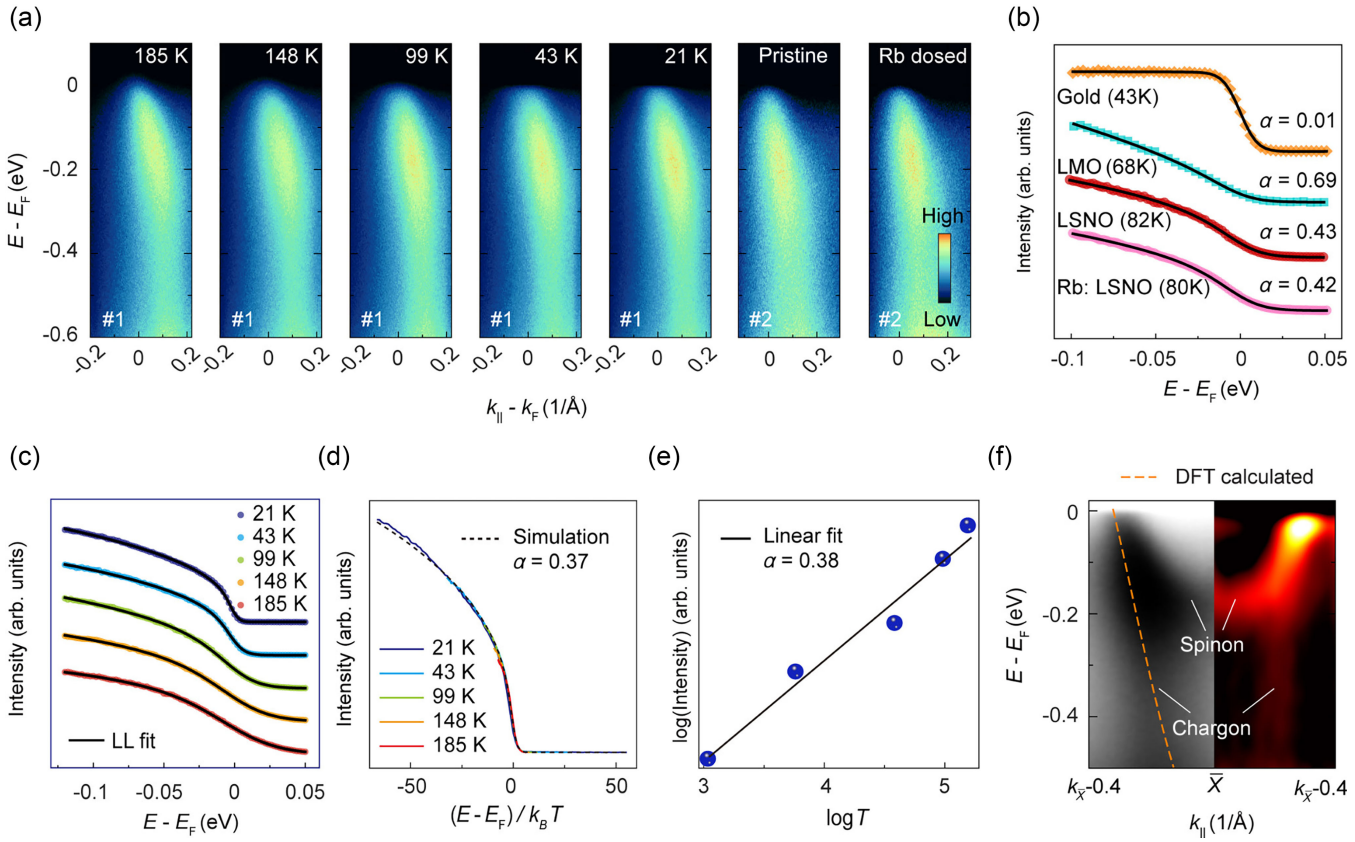


FIG. 4. Non-Fermi-liquid behavior of $La_{1.4}Sr_{0.6}NiO_4$. (a) ARPES measurements of the band dispersion along $\bar{\Gamma}\bar{M}$ at selected temperatures using an LH-polarized laser at 7 eV. Temperature-dependent data and Rb-doping-dependent data were collected from samples no. 1 and no. 2, respectively. (b) Comparison of integrated energy-distribution curves (EDCs) of polycrystalline gold, $Li_{0.9}Mo_6O_{17}$ and $La_{1.4}Sr_{0.6}NiO_4$ before and after Rb doping with LL exponent indicated. (c) Integrated EDCs of $La_{1.4}Sr_{0.6}NiO_4$ measured at different temperatures and the fits to the LL model. (d) Scaling plot of the EDCs in (c) with a scaling factor of $T^{0.37}$ (see the main text for details). The dashed line plots the simulated LL spectral function with anomalous exponent $\alpha = 0.37$. (e) Log-log plot of the EDC intensity at E_F versus the temperature. The black line is a linear fit to the data with $\alpha = 0.38$. (f) Spectroscopic evidence of the spin-charge separation. Left: raw data measured at $\bar{X}$ along the red line in Fig. 2(b). The orange dashed line is the DFT-calculated band dispersion. Only one band is predicted by the calculation. Right: the curvature plot of the spectra. Two bands are clearly observed. Data were measured using 51-eV photons with LH polarization at 15 K.

III. DISCUSSION

The observation of LL behavior in a strongly correlated square lattice is beyond expectation, as the LL model is typically restricted to quasi-1D systems. While LL physics has been reported in other quasi-two-dimensional materials, those systems usually feature quasi-1D structural motifs [33,65]. In η-Mo_4O_{11}, for example, LL physics is preserved by orthogonal orbital components along different chain directions. This scenario, however, is not applicable to $La_{1.4}Sr_{0.6}NiO_4$, where the LL behavior emerges within an intrinsically two-dimensional Ni-O plane, and the electrons along orthogonal directions exhibit mixed orbital characters. On the other hand, although single-layer nickelates are well known to exhibit stripelike states [49], there is no clear evidence for such orders in $La_{2-x}Sr_xNiO_4$ at doping levels $x > 0.5$, and the relationship between the stripe order and the LL phase remains unclear.

Remarkably, our observation closely conforms to the theoretical model of square Fermi surfaces [34–36]. The square geometry of the Fermi surface suggests that nearest-neighbor hopping dominates the low-energy electronic structure. This is consistent with the tight-binding model on a square lattice, where the Fermi surface becomes perfectly nested in the absence of further-neighbor hopping. Our DFT calculations and ARPES measurements both indicate that the electronic bands near the Fermi level are primarily derived from the Ni $d_{x^2-y^2}$ and d_{z^2} orbitals, with hopping integrals dominated by nearest-neighbor terms (see Supplemental Material for details about the hopping integrals extracted through Wannier simulation of the band structure [50]). This simple model nicely captures the essential quasi-1D character of the electronic excitations, facilitating the mapping of the square lattice to effective one-dimensional chains along orthogonal directions [34–36]. Within this framework, the bosonic

component of electron-electron interactions destabilizes the conventional Fermi-liquid phase, giving rise to LL behavior. Moreover, theoretical studies have shown that for repulsive Hubbard interactions on a square lattice with perfect nesting, density-wave instabilities (e.g., spin or charge-density waves) are favored. Our findings in $La_{1.4}Sr_{0.6}NiO_4$ are consistent with this picture: the system exhibits strong correlations and a tendency toward density-wave order, as hinted by the kink in the resistivity under pressure.

Our findings in the single-layer nickelate $La_{1.4}Sr_{0.6}NiO_4$ also provide important insights into the physics of nickelates. On the one hand, the experiment isolates the intralayer and interlayer electron correlation effect. A comparison of the electronic structures across single- and multilayer nickelates suggests that intralayer correlation effects generate similar waterfall features in the $d_{x^2-y^2}$ band dispersions, whereas interlayer correlation effects further renormalize the bandwidth, Fermi velocity, and carrier effective mass in multilayer nickelates [54]. Consistent with the previous theoretical proposal [51], this result suggests a dominant role of the interlayer electron correlation effect in the physics of multilayer nickelates. On the other hand, bilayer and trilayer nickelates exhibit rounded Fermi surfaces due to interlayer hopping, which suppresses the LL behavior. This warping disrupts the perfect nesting condition inherent in the square Fermi surface, which tends to suppress density-wave instabilities and may favor superconducting pairing [34–36]. This picture resonates with Anderson's proposal that the unconventional superconductivity is possibly associated with the LL-like physics in higher dimensions. These results also provide a possible understanding of the non-Fermi-liquid behavior observed in RP-phase nickelates: although the LL behavior within the Ni-O layer is suppressed by the interlayer coupling, it may still affect the electronic behavior in multilayer nickelates.

In conclusion, our comprehensive investigation of $La_{1.4}Sr_{0.6}NiO_4$ elucidates its electronic structure and correlation effects. Our ARPES measurements reveal spectral characteristics consistent with LL behavior in $La_{1.4}Sr_{0.6}NiO_4$. By isolating the physics of the single Ni-O layer, our work not only provides important insights into the novel electronic behaviors in nickelates but also highlights the delicate interplay between dimensionality and electronic instabilities in correlated materials.

IV. METHODS

A. ARPES experiment

Single crystals of $La_{1.4}Sr_{0.6}NiO_4$ were grown by the high-pressure optical floating zone technique. Synchrotron-based ARPES measurements were conducted at beamline 5-2 of the Stanford Synchrotron Radiation Lightsource under Proposal No. S-XV-ST-6370. The samples were cleaved *in situ* under ultrahigh vacuum below 5×10^{-11} mbar. Data were collected with a Scienta DA30 electron analyzer. The total energy and angular resolutions were set to 15 meV and 0.2°, respectively. Preliminary data were collected at beamline Bloch (Proposal No. 20230668) in MAX IV, beamline 03U (Proposal No. 2025-SSRF-PT-513724), and beamline 09U (Proposal No. 2025-SSRF-PT-512611) in the Shanghai Synchrotron Radiation Facility, and beamline 10.0.1 (Proposal No. ALS-11649) in the Advanced Light Source.

Laser-based ARPES measurements were conducted at Tsinghua University. The 7-eV laser was delivered by frequency doubling in a potassium beryllium fluoroborate (KBBF) crystal and then focused on the sample with a beam spot of about $10 \times 10\ \mu m^2$. Samples were cleaved *in situ* under ultrahigh vacuum below 6×10^{-11} mbar. Data were collected with a Scienta DA30 electron analyzer. The total energy and angular resolutions were set to 3 meV and 0.2°, respectively.

B. DFT + DMFT calculations

The DFT calculations were performed using the WIEN2K package [66]. We simulate the Sr-doping effect by reducing the total valence electrons and compensating it by a uniform background of negative charges in DFT. We perform fully charge-self-consistent single-site DFT + DMFT calculations using the DFT + eDMFT code developed by Haule *et al.* [67,68] based on WIEN2K. We choose a large hybridization energy window from −10 to 10 eV. All five Ni-3*d* orbitals are considered as correlated ones, and a local Coulomb interaction Hamiltonian with Ising form is used, which is parametrized by on-site Hubbard U and Hund's coupling J_H. We choose the nominal double-counting scheme with a nominal Ni-3*d* occupancy of 7.4 electrons corresponding to the Sr doping of $x = 0.6$. The continuous- time quantum Monte Carlo [69] is used as an impurity solver, and a total of 2.56×10^9 samplings are performed. The self-energy on the real frequency is obtained by the analytical continuation method of maximum entropy. All calculations are performed at 100 K. We use the WANNIER90 package [70] to construct a tight-binding model consisting of Ni $d_{x^2-y^2}$ and d_{z^2} orbitals for a monolayer $La_{1.4}Sr_{0.6}NiO_4$.

ACKNOWLEDGMENTS

This work is funded by the National Key R&D Program of China (Grants No. 2022YFA1403100 and No. 2022YFA1403201), the National Natural Science Foundation of China (Grants No. 12274251, No. 12004270, No. 52272265, and No. 12174365). L. X. Y. acknowledges support from the Tsinghua University Initiative Scientific Research Program and the Fund of Science and Technology on Surface Physics and Chemistry Laboratory (Grant No. XKFZ202102). Y. L. W. acknowledges support from the Innovation Program

for Quantum Science and Technology (Grant No. 2021ZD0302803) and the New Cornerstone Science Foundation. Use of the Stanford Synchrotron Radiation Light Source, SLAC National Accelerator Laboratory, is supported by the U.S. Department of Energy, Office of Science, Office of Basic Energy Sciences under Contract No. DE-AC02-76SF00515. This research used resources of the Advanced Light Source, a U.S. DOE Office of Science User Facility under Contract No. DE-AC02-05CH11231.

DATA AVAILABILITY

The data that support the findings of this study are available from the corresponding author upon request.

[1] W. E. Pickett, *The dawn of the nickel age of superconductivity*, Nat. Rev. Phys. **3**, 7 (2021).
[2] D. Li, K. Lee, B. Y. Wang, M. Osada, S. Crossley, H. R. Lee, Y. Cui, Y. Hikita, and H. Y. Hwang, *Superconductivity in an infinite-layer nickelate*, Nature (London) **572**, 624 (2019).
[3] G. A. Pan *et al.*, *Superconductivity in a quintuple-layer square-planar nickelate*, Nat. Mater. **21**, 160 (2022).
[4] A. S. Botana and M. R. Norman, *Similarities and differences between* $LaNiO_2$ *and* $CaCuO_2$ *and implications for superconductivity*, Phys. Rev. X **10**, 011024 (2020).
[5] B. Y. Wang, K. Lee, and B. H. Goodge, *Experimental progress in superconducting nickelates*, Annu. Rev. Condens. Matter Phys. **15**, 305 (2024).
[6] X. Ding *et al.*, *Critical role of hydrogen for superconductivity in nickelates*, Nature (London) **615**, 50 (2023).
[7] Q. Gu and H.-H. Wen, *Superconductivity in nickel-based 112 systems*, Innovation **3**: 100202 (2022).
[8] H. Sun, M. Huo, X. Hu, J. Li, Z. Liu, Y. Han, L. Tang, Z. Mao, P. Yang, B. Wang, J. Cheng, D.-X. Yao, G.-M. Zhang, and M. Wang, *Signatures of superconductivity near 80 K in a nickelate under high pressure*, Nature (London) **621**, 493 (2023).
[9] N. Wang *et al.*, *Bulk high-temperature superconductivity in pressurized tetragonal* $La_2PrNi_2O_7$, Nature (London) **634**, 579 (2024).
[10] Y. Zhang, D. Su, Y. Huang, Z. Shan, H. Sun, M. Huo, K. Ye, J. Zhang, Z. Yang, Y. Xu, Y. Su, R. Li, M. Smidman, M. Wang, L. Jiao, and H. Yuan, *High-temperature superconductivity with zero resistance and strange-metal behaviour in* $La_3Ni_2O_{7-\delta}$, Nat. Phys. **20**, 1269 (2024).
[11] Y. Zhu *et al.*, *Superconductivity in pressurized trilayer* $La_4Ni_3O_{10-\delta}$ *single crystals*, Nature (London) **631**, 531 (2024).
[12] M. Zhang *et al.*, *Superconductivity in trilayer nickelate* $La_4Ni_3O_{10}$ *under pressure*, Phys. Rev. X **15**, 021005 (2025).
[13] E. K. Ko, Y. Yu, Y. Liu, L. Bhatt, J. Li, V. Thampy, C.-T. Kuo, B. Y. Wang, Y. Lee, K. Lee, J.-S. Lee, B. H. Goodge, D. A. Muller, and H. Y. Hwang, *Signatures of ambient pressure superconductivity in thin film* $La_3Ni_2O_7$, Nature (London) **638**, 935 (2025).
[14] G. Zhou, W. Lv, H. Wang, Z. Nie, Y. Chen, Y. Li, H. Huang, W.-Q. Chen, Y.-J. Sun, Q.-K. Xue, and Z. Chen, *Ambient-pressure superconductivity onset above 40 K in* $(La,Pr)_3Ni_2O_7$ *films*, Nature (London) **640**, 641 (2025).
[15] J. Li, D. Peng, P. Ma, H. Zhang, Z. Xing, X. Huang, C. Huang, M. Huo, D. Hu, Z. Dong, X. Chen, T. Xie, H. Dong, H. Sun, Q. Zeng, H.-k. Mao, and M. Wang, *Identification of superconductivity in bilayer nickelate* $La_3Ni_2O_7$ *under high pressure up to 100 GPa*, Nat. Sci. Rev. **12**, nwaf220 (2025).
[16] Y. Wang, K. Jiang, J. Ying, T. Wu, J. Cheng, J. Hu, and X. Chen, *Recent progress in nickelate superconductors*, Nat. Sci. Rev. **12**, nwaf373 (2025).
[17] M. Wang, H.-H. Wen, T. Wu, D.-X. Yao, and T. Xiang, *Normal and superconducting properties of* $La_3Ni_2O_7$, Chin. Phys. Lett. **41**, 077402 (2024).
[18] Y. Li and L. Yang, *Electronic structure and ultrafast dynamics of nickel-based high-temperature superconductors*, Acta Phys. Sin. **74**, 177402 (2025).
[19] Seiichiro Onari, Daisuke Inoue, Rina Tazai, Youichi Yamakawa, and H. Kontani, *Impact of multiband effects on non-Fermi-liquid transport phenomena in bilayer nickelates*, Phys. Rev. B **113**, 245110 (2026).
[20] J.-X. Wang, Z. Ouyang, R.-Q. He, and Z.-Y. Lu, *Non-Fermi liquid and Hund correlation in* $La_4Ni_3O_{10}$ *under high pressure*, Phys. Rev. B **109**, 165140 (2024).
[21] Z. Liu, M. Huo, J. Li, Q. Li, Y. Liu, Y. Dai, X. Zhou, J. Hao, Y. Lu, M. Wang, and H.-H. Wen, *Electronic correlations and partial gap in the bilayer nickelate* $La_3Ni_2O_7$, Nat. Commun. **15**, 7570 (2024).
[22] Y. Li *et al.*, *Distinct ultrafast dynamics of bilayer and trilayer nickelate superconductors regarding the density-wave-like transitions*, Sci. Bull. **70**, 180 (2025).
[23] Y. Li, X. Du, Y. Cao, C. Pei, M. Zhang, W. Zhao, K. Zhai, R. Xu, Z. Liu, Z. Li, J. Zhao, G. Li, Y. Qi, H. Guo, Y. Chen, and L. Yang, *Electronic correlation and pseudogap-like behavior of high-temperature superconductor* $La_3Ni_2O_7$, Chin. Phys. Lett. **41**, 087402 (2024).
[24] F. Lechermann, J. Gondolf, S. Bötzel, and I. M. Eremin, *Electronic correlations and superconducting instability in* $La_3Ni_2O_7$ *under high pressure*, Phys. Rev. B **108**, L201121 (2023).
[25] Y. Chen, Y.-H. Tian, J.-M. Wang, R.-Q. He, and Z.-Y. Lu, *Non-Fermi liquid and antiferromagnetic correlations with hole doping in the bilayer two-orbital Hubbard model of* $La_3Ni_2O_7$ *at zero temperature*, Phys. Rev. B **110**, 235119 (2024).
[26] E. Zhang, D. Peng, Y. Zhu, L. Chen, B. Cui, X. Wang, W. Wang, Q. Zeng, and J. Zhao, *Bulk superconductivity in pressurized trilayer nickelate* $Pr_4Ni_3O_{10}$ *single crystals*, Phys. Rev. X **15**, 021008 (2025).
[27] J. Yang *et al.*, *Orbital-dependent electron correlation in double-layer nickelate* $La_3Ni_2O_7$, Nat. Commun. **15**, 4373 (2024).
[28] H. Li, X. Zhou, T. Nummy, J. Zhang, V. Pardo, W. E. Pickett, J. F. Mitchell, and D. S. Dessau, *Fermiology and electron dynamics of trilayer nickelate* $La_4Ni_3O_{10}$, Nat. Commun. **8**, 704 (2017).
[29] S. Abadi, K.-J. Xu, E. G. Lomeli, P. Puphal, M. Isobe, Y. Zhong, A. V. Fedorov, S.-K. Mo, M. Hashimoto, D.-H. Lu, B. Moritz, B. Keimer, T. P. Devereaux, M. Hepting, and Z.-X. Shen, *Electronic structure of the alternating*

monolayer-trilayer phase of $La_3Ni_2O_7$, Phys. Rev. Lett. **134**, 126001 (2025).

[30] R. Eguchi, A. Chainani, M. Taguchi, M. Matsunami, Y. Ishida, K. Horiba, Y. Senba, H. Ohashi, and S. Shin, *Fermi surfaces, electron-hole asymmetry, and correlation kink in a three-dimensional Fermi liquid* $LaNiO_3$, Phys. Rev. B **79**, 115122 (2009).

[31] P. D. C. King, H. I. Wei, Y. F. Nie, M. Uchida, C. Adamo, S. Zhu, X. He, I. Božović, D. G. Schlom, and K. M. Shen, *Atomic-scale control of competing electronic phases in ultrathin* $LaNiO_3$, Nat. Nanotechnol. **9**, 443 (2014).

[32] L. Kang *et al.*, *Band-selective Holstein polaron in Luttinger liquid material* $A_{0.3}MoO_3$ *(*A = K*, Rb)*, Nat. Commun. **12**, 6183 (2021).

[33] X. Du, L. Kang, Y. Y. Lv, J. S. Zhou, X. Gu, R. Z. Xu, Q. Q. Zhang, Z. X. Yin, W. X. Zhao, Y. D. Li, S. M. He, D. Pei, Y. B. Chen, M. X. Wang, Z. K. Liu, Y. L. Chen, and L. X. Yang, *Crossed Luttinger liquid hidden in a quasi-two-dimensional material*, Nat. Phys. **19**, 40 (2023).

[34] A. Luther, *Interacting electrons on a square Fermi surface*, Phys. Rev. B **50**, 11446 (1994).

[35] A. T. Zheleznyak, V. M. Yakovenko, and I. E. Dzyaloshinskii, *Parquet solution for a flat Fermi surface*, Phys. Rev. B **55**, 3200 (1997).

[36] J. O. Fjærestad, A. Sudbø, and A. Luther, *Correlation functions for a two-dimensional electron system with bosonic interactions and a square Fermi surface*, Phys. Rev. B **60**, 13361 (1999).

[37] P. W. Anderson, *Breaking the log-jam in many-body physics: Fermi surfaces without Fermi liquids*, Phys. Scr. T **42**, 11 (1992).

[38] P. W. Anderson, *"Luttinger-liquid" behavior of the normal metallic state of the 2D Hubbard model*, Phys. Rev. Lett. **64**, 1839 (1990).

[39] P. W. Anderson, *Experimental constraints on the theory of high-*T_c *superconductivity*, Science **256**, 1526 (1992).

[40] A. Yu. Zavidonov and D. Brinkmann, *Magnetic properties of chains in cuprate superconductors studied by the Luttinger-liquid model*, Phys. Rev. B **61**, 3282 (2000).

[41] M. Hücker, K. Chung, M. Chand, T. Vogt, J. M. Tranquada, and D. J. Buttrey, *Oxygen and strontium codoping of* La_2NiO_4*: Room-temperature phase diagrams*, Phys. Rev. B **70**, 064105 (2004).

[42] Z. Luo, X. Hu, M. Wang, W. Wú, and D.-X. Yao, *Bilayer two-orbital model of* $La_3Ni_2O_7$ *under pressure*, Phys. Rev. Lett. **131**, 126001 (2023).

[43] X. Du *et al.*, *Dichotomy in low- and high-energy band renormalizations in trilayer nickelate* $La_4Ni_3O_{10}$*: A comparison with cuprates*, Phys. Rev. Lett. **135**, 146506 (2025).

[44] X.-Z. Qu, D.-W. Qu, J. Chen, C. Wu, F. Yang, W. Li, and G. Su, *Bilayer t-J-*$J_\perp$ *model and magnetically mediated pairing in the pressurized nickelate* $La_3Ni_2O_7$, Phys. Rev. Lett. **132**, 036502 (2024).

[45] C. Lu, Z. Pan, F. Yang, and C. Wu, *Interlayer-coupling-driven high-temperature superconductivity in* $La_3Ni_2O_7$ *under pressure*, Phys. Rev. Lett. **132**, 146002 (2024).

[46] Y. F. Yang, G.-M. Zhang, and F.-C. Zhang, *Interlayer valence bonds and two-component theory for high-*T_c *superconductivity of* $La_3Ni_2O_7$ *under pressure*, Phys. Rev. B **108**, L201108 (2023).

[47] H. Sakakibara, N. Kitamine, M. Ochi, and K. Kuroki, *Possible high* T_c *superconductivity in* $La_3Ni_2O_7$ *under high pressure through manifestation of a nearly half-filled bilayer Hubbard model*, Phys. Rev. Lett. **132**, 106002 (2024).

[48] H. Yoshizawa, T. Kakeshita, R. Kajimoto, T. Tanabe, T. Katsufuji, and Y. Tokura, *Stripe order at low temperatures in* $La_{2-x}Sr_xNiO_4$ *with* $0.289 \lesssim x \lesssim 0.5$, Phys. Rev. B **61**, R854 (2000).

[49] R. Kajimoto, K. Ishizaka, H. Yoshizawa, and Y. Tokura, *Spontaneous rearrangement of the checkerboard charge order to stripe order in* $La_{1.5}Sr_{0.5}NiO_4$, Phys. Rev. B **67**, 014511 (2003).

[50] See Supplemental Material at http://link.aps.org/supplemental/10.1103/744w-ln1x for details of (i) the estimation of band renormalization factor, (ii) calculated constant-energy contours at different binding energies, (iii) calculated band structure and Fermi surface at different doping levels, (iv) experimental Fermi surface measured at selected photon energies, (v) methodology of the self-energy extraction, (vi) self-energy analysis using laser ARPES, (vii) DMFT calculation of electron spectral function, (viii) two-orbital Wannier simulation, (ix) temperature evolution of the Luttinger-liquid anomalous exponent, (x) line-shape analysis across different momentum cuts, and (xi) ultrafast reflectivity measurement.

[51] S. Ryee, N. Witt, and T. O. Wehling, *Quenched pair breaking by interlayer correlations as a key to superconductivity in* $La_3Ni_2O_7$, Phys. Rev. Lett. **133**, 096002 (2024).

[52] B. P. Xie *et al.*, *High-energy scale revival and giant kink in the dispersion of a cuprate superconductor*, Phys. Rev. Lett. **98**, 147001 (2007).

[53] B. Moritz, F. Schmitt, W. Meevasana, S. Johnston, E. M. Motoyama, M. Greven, D. H. Lu, C. Kim, R. T. Scalettar, Z. X. Shen, and T. P. Devereaux, *Effect of strong correlations on the high energy anomaly in hole- and electron-doped high-Tc superconductors*, New J. Phys. **11**, 093020 (2009).

[54] J. Krsnik and K. Held, *Local correlations necessitate waterfalls as a connection between quasiparticle band and developing Hubbard bands*, Nat. Commun. **16**, 255 (2025).

[55] T. Valla, T. E. Kidd, W. G. Yin, G. D. Gu, P. D. Johnson, Z. H. Pan, and A. V. Fedorov, *High-energy kink observed in the electron dispersion of high-temperature cuprate superconductors*, Phys. Rev. Lett. **98**, 167003 (2007).

[56] Y. Liu *et al.*, *Anomalous high-energy waterfall-like electronic structure in 5d transition metal oxide* Sr_2IrO_4 *with a strong spin-orbit coupling*, Sci. Rep. **5**, 13036 (2015).

[57] X. Gu *et al.*, *Robust kagome electronic structure in the topological quantum magnets* XMn_6Sn_6 *(*X = Dy*, Tb, Gd, Y)*, Phys. Rev. B **105**, 155108 (2022).

[58] J. S. Zhou, R. Z. Xu, X. Q. Yu, F. J. Cheng, W. X. Zhao, X. Du, S. Z. Wang, Q. Q. Zhang, X. Gu, S. M. He, Y. D. Li, M. Q. Ren, X. C. Ma, Q. K. Xue, Y. L. Chen, C. L. Song, and L. X. Yang, *Evidence for band renormalizations in strong-coupling superconducting alkali-fulleride films*, Phys. Rev. Lett. **130**, 216004 (2023).

[59] M. H. Chang, S. Backes, D. Lu, N. Gauthier, M. Hashimoto, G. Y. Chen, H. H. Wen, S. K. Mo, R. Valentí, and H. Pfau, *Dispersion kinks from electronic correlations in an unconventional iron-based superconductor*, Nat. Commun. **15**, 9958 (2024).

[60] F. Wang, J. V. Alvarez, S. K. Mo, J. W. Allen, G. H. Gweon, J. He, R. Jin, D. Mandrus, and H. Höchst, *New Luttinger-liquid physics from photoemission on* $Li_{0.9}Mo_6O_{17}$, Phys. Rev. Lett. **96**, 196403 (2006).

[61] J. Graf, G. H. Gweon, K. McElroy, S. Y. Zhou, C. Jozwiak, E. Rotenberg, A. Bill, T. Sasagawa, H. Eisaki, S. Uchida, H. Takagi, D. H. Lee, and A. Lanzara, *Universal high energy anomaly in the angle-resolved photoemission spectra of high temperature superconductors: Possible evidence of spinon and holon branches*, Phys. Rev. Lett. **98**, 067004 (2007).

[62] B. J. Kim, H. Koh, E. Rotenberg, S. J. Oh, H. Eisaki, N. Motoyama, S. Uchida, T. Tohyama, S. Maekawa, Z. X. Shen, and C. Kim, *Distinct spinon and holon dispersions in photoemission spectral functions from one-dimensional SrCuO2*, Nat. Phys. **2**, 397 (2006).

[63] Y. Ma, H. C. Diaz, J. Avila, C. Chen, V. Kalappattil, R. Das, M.-H. Phan, T. Čadež, J. M. P. Carmelo, M. C. Asensio, and M. Batzill, *Angle resolved photoemission spectroscopy reveals spin charge separation in metallic MoSe2 grain boundary*, Nat. Commun. **8**, 14231 (2017).

[64] J. Hyun, Y. Lee, C. Y. Lim, G. Lee, J. Cha, Y. Ahn, M. Jho, S. Gim, M. Park, M. Hashimoto, D. Lu, Y. Kim, and S. Kim, *Band-selective spin-charge separation across the charge density wave transition in quasi-1D* $NbSe_3$, Phys. Rev. Lett. **134**, 206402 (2025).

[65] P. Wang, G. Yu, Y. H. Kwan, Y. Jia, S. Lei, S. Klemenz, F. A. Cevallos, R. Singha, T. Devakul, K. Watanabe, T. Taniguchi, S. L. Sondhi, R. J. Cava, L. M. Schoop, S. A. Parameswaran, and S. Wu, *One-dimensional Luttinger liquids in a two-dimensional moiré lattice*, Nature (London) **605**, 57 (2022).

[66] P. Blaha, K. Schwarz, F. Tran, R. Laskowski, G. K. H. Madsen, and L. D. Marks, *WIEN2K: An APW + lo program for calculating the properties of solids*, J. Chem. Phys. **152**, 074101 (2020).

[67] K. Haule, C.-H. Yee, and K. Kim, *Dynamical mean-field theory within the full-potential methods: Electronic structure of* $CeIrIn_5$, $CeCoIn_5$, *and* $CeRhIn_5$, Phys. Rev. B **81**, 195107 (2010).

[68] K. Haule and T. Birol, *Free energy from stationary implementation of the* DFT + DMFT *functional*, Phys. Rev. Lett. **115**, 256402 (2015).

[69] E. Gull, A. J. Millis, A. I. Lichtenstein, A. N. Rubtsov, M. Troyer, and P. Werner, *Continuous-time Monte Carlo methods for quantum impurity models*, Rev. Mod. Phys. **83**, 349 (2011).

[70] A. A. Mostofi, J. R. Yates, Y.-S. Lee, I. Souza, D. Vanderbilt, and N. Marzari, *WANNIER90: A tool for obtaining maximally-localised Wannier functions*, Comput. Phys. Commun. **178**, 685 (2008).